Biochimica et Biophysica Acta 1848 (2015) 1081–1091

Contents lists available at ScienceDirect

Biochimica et Biophysica Acta

journal homepage: www.elsevier.com/locate/bbamem

Helical cationic antimicrobial peptide length and its impact on membrane disruption

Melanie L. Juba [a], Devin K. Porter [a,1], Elissa H. Williams [a,b], Carlos A. Rodriguez [a], Stephanie M. Barksdale [c], Barney M. Bishop [a,*]

[a] Department of Chemistry and Biochemistry, George Mason University, 4400 University Dr., Fairfax, VA 22030, USA
[b] Material Measurement Laboratory, National Institute of Science and Technology, 100 Bureau Dr., Gaithersburg, MD 20899, USA
[c] School of Systems Biology, George Mason University, 10900 University Blvd., Manassas, VA 20110, USA

ARTICLE INFO

Article history:
Received 6 August 2014
Received in revised form 31 December 2014
Accepted 11 January 2015
Available online 3 February 2015

Keywords:
Antimicrobial peptides
Stereochemistry
Scanning electron microscopy
Membrane depolarization
Membrane permeabilization
Cathelicidins

ABSTRACT

Cationic antimicrobial peptides (CAMPs) are important elements of innate immunity in higher organisms, representing an ancient defense mechanism against pathogenic bacteria. These peptides exhibit broad-spectrum antimicrobial activities, utilizing mechanisms that involve targeting bacterial membranes. Recently, a 34-residue CAMP (NA-CATH) was identified in cDNA from the venom gland of the Chinese cobra (*Naja atra*). A semi-conserved 11-residue pattern observed in the NA-CATH sequence provided the basis for generating an 11-residue truncated peptide, ATRA-1A, and its corresponding D-peptide isomer. While the antimicrobial and biophysical properties of the ATRA-1A stereoisomers have been investigated, their modes of action remain unclear. More broadly, mechanistic differences that can arise when investigating minimal antimicrobial units within larger naturally occurring CAMPs have not been rigorously explored. Therefore, the studies reported here are focused on this question and the interactions of full-length NA-CATH and the truncated ATRA-1A isomers with bacterial membranes. The results of these studies indicate that in engineering the ATRA-1A isomers, the associated change in peptide length and charge dramatically impacts not only their antimicrobial effectiveness, but also the mechanism of action they employ relative to that of the full-length parent peptide NA-CATH. These insights are relevant to future efforts to develop shorter versions of larger naturally occurring CAMPs for potential therapeutic applications.

1. Introduction

Cationic antimicrobial peptides (CAMPs) are pervasive in nature and represent an evolutionarily ancient mechanism for defending against invading microorganisms. These peptides exhibit broad spectrum antimicrobial effectiveness and are important elements of innate immunity, which provide the first line of defense against infection. Despite their widespread use, they exhibit limited bacterial resistance [1]. These qualities provide CAMPs an advantage over conventional therapeutics for fighting infections. Although CAMPs offer great potential as the basis for a new class of antibiotics, many of the details of the mechanisms by which they exert their antimicrobial effects remain unclear. Greater understanding of the relationship between CAMP physico-chemical properties and antimicrobial action is needed in order to realize their therapeutic potential.

CAMPs have been shown to interact with bacterial membranes and in many cases induce membrane disruption [2]. However, these interactions appear to be complex and the correlations between peptide physico-chemical properties, membrane composition and modes of action are poorly understood. CAMPs are usually amphipathic peptides presenting discrete cationic and hydrophobic surfaces. The spatial partitioning of these surfaces allows favorable electrostatic interaction with negatively charged lipid head groups on the outer surface of bacterial membranes and insertion into the hydrophobic interior of the bilayer, leading ultimately to membrane disruption [3,4]. Widely accepted membrane disruption mechanisms range from the "barrel-stave" model to the "carpet model". In the "barrel-stave" model, amphipathic helical peptides insert into the bacterial membrane, forming peptide lined structures with large central pores [2,5,6]. A similar proposed model is the "toroidal pore" where amphipathic helical peptides insert into the lipid membrane and form less defined transient supramolecular pores [5–7]. In the "carpet model," the peptides gather and concentrate at the membrane surface, interacting with the anionic lipid head groups, until the peptide concentration threshold is reached. This results in distortions in the lipid bilayer curvature and formation of transient gaps in the membrane [2,5,6].

* Corresponding author at: Department of Chemistry and Biochemistry, George Mason University, 4400 University Drive, 3E2, Fairfax, VA 22030, USA. Tel.: +7039938302.
E-mail address: bbishop1@gmu.edu (B.M. Bishop).
[1] Present address: Devin K. Porter, National Institute of Environmental Health Sciences, Research Triangle Park, NC, USA.

http://dx.doi.org/10.1016/j.bbamem.2015.01.007
0005-2736/

NA-CATH

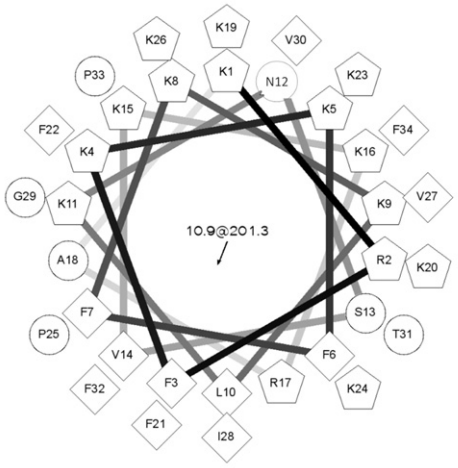

Sequence	KRFKKFFKKLKNSVKKRAKK FFKKPKVIGVTFPF
Length (res)	34
Net Charge	+15

ATRA-1A

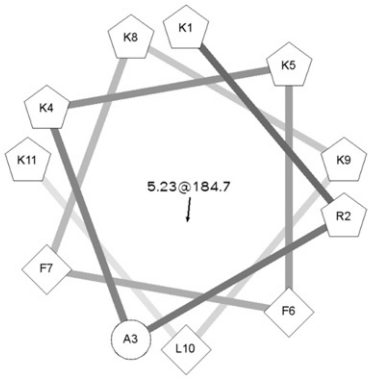

Sequence	KRAKKFFKKLK-NH_2
Length (res)	11
Net Charge	+ 8

Fig. 1. Helical wheel projection* and peptide sequences with associated net charge. The helical wheel projections of NA-CATH (left) and ATRA-1A (right) display hydrophilic residues as circles, hydrophobic residues as diamonds and positively charged residues as pentagons with the hydrophobic moment denoted in the center. Below the helical wheel projections are tables containing peptide sequence, length and charge information. The ATRA motifs are shaded gray in the NA-CATH sequence with the residues that differ between the motifs underlined. * Generated using http://rzlab.ucr.edu/scripts/wheel/wheel.cgi.

CAMPs can be grouped into families based on multiple factors, such as evolutionary relationships, conserved sequence patterns and structural elements. Cathelicidins are a sequence diverse family of vertebrate CAMPs that have been identified based on the highly conserved cathelin domain present in the precursor protein [8–11]. Recently, the sequence of a 34-residue helical cathelicidin, NA-CATH, was identified from cDNA derived from the venom glands of the elapid snake, *Naja atra* [12,13]. Analysis of the NA-CATH sequence revealed a semi-conserved 11-residue repeated sequence pattern. The 11-residue peptide amide, ATRA-1A, was designed based on this pattern (Fig. 1) [14]. Furthermore, the D-isomer of ATRA-1A was also investigated because D-peptide isomers have been shown to be more resistant to proteases than the corresponding L-peptides, which could enhance a peptide's therapeutic utility [15–17]. Significant disparities were observed in the antimicrobial effectiveness of the ATRA-1A stereoisomers [15]. Moreover, circular dichroism studies noted subtle dissimilarities in the structural properties of the peptide isomers in the presence of model anionic membranes, and differences in their abilities to disrupt model membranes and induce aggregation became evident in turbidity studies and fluorescence microscopy. While these studies focused on subtle differences in the properties of the ATRA-1A peptide isomers and their interactions with model membranes, they did not consider full-length NA-CATH, and how its properties may compare to those of the shorter ATRA-1A isomers.

The present study focuses on mechanistic differences that may arise when studying full-length CAMPs and antimicrobially active truncated versions of the peptide in order to identify minimal peptide units retaining antimicrobial activity and regions of the larger peptides responsible for their antimicrobial activity. We have investigated the full-length CAMP NA-CATH and the L- and D-isomers of the truncated peptide ATRA-1A in order to explore how altering CAMP length can affect antimicrobial activity and interaction with bacterial membranes. Specifically, we aim to more clearly elucidate similarities and differences in the membrane disruption mechanisms employed by full-length NA-CATH and the ATRA-1A isomers by focusing on key aspects of peptide-induced membrane disruption and antimicrobial kinetics in high and low salt environments against *Escherichia coli* and *Bacillus cereus*.

2. Material and methods

2.1. Materials

The peptides used in these studies were custom synthesized by AAPPTEC, LLC (Louisville, KY).[2] The supplier reported purities of NA-CATH, L-ATRA-1A and D-ATRA-1A were 95.0%, 95.2% and 95.4%, respectively, based on high-performance liquid chromatography (HPLC) analysis of the purified peptides. The bacterial strains of *Escherichia* (*E.*) *coli* (ATCC# 25922) and *Bacillus* (*B.*) *cereus* (ATCC# 11778) used in these studies were purchased from the American Type Culture Collection (Manassas, VA). 3,3′-dipropylthiacarbocyanine ($diSC_3$-(5)) was purchased from AnaSpec (Fremont, CA). SYTOX Green was purchased from Invitrogen (Carlsbad, CA). Mueller Hinton Broth (MHB) was purchased from Becton Dickinson and Company (Sparks, MD). 4-(2-Hydroxyethyl)-1-piperazine ethane sulfonic acid (HEPES) was purchased from Acros Organics (New Jersey, US). Phosphate buffered saline (PBS) was purchased from Corning-cellgro (Manassas, VA). Resazurin, sodium salt was purchased from Sigma-Aldrich (St. Louis, MO). A SpectraMax Gemini EM was used for all experiments utilizing a plate-reading fluorimeter (Molecular Devices, Sunnyvale, CA).

2.2. Antimicrobial activity

The antimicrobial performances of NA-CATH, L-ATRA-1A and D-ATRA-1A were determined using a resazurin-based assay [18,19]. Frozen enumerated bacterial aliquots were thawed on ice and gently mixed.

[2] Commercial equipment and material suppliers are identified in this paper to adequately describe experimental procedures. This does not imply endorsement by NIST.

For each strain, bacteria were diluted to 2×10^6 CFU/mL in low salt buffer (10 mM phosphate buffer, pH 7.4) or high salt buffer (10 mM phosphate buffer, 100 mM KCl, pH 7.4) and added in 50 μL aliquots to the wells of a black 96-well microtiter plate containing serially diluted peptide (50 μL) dissolved in the same buffer. In these assays control wells were prepared containing bacteria with no peptide. The microtiter plate was incubated for 3 h at 37 ° C (*E. coli*) or 30 ° C (*B. cereus*). After 3 h, 100 μL of PBS solution with dissolved resazurin and MHB was added to the wells of the microtiter plate. The amounts of resazurin and MHB used were dependent on bacterial strain, with the final resazurin/MHB concentrations (w/v) being 100 μM resazurin/0.2% for *E. coli* and 12.5 μM resazurin/0.05% for *B. cereus*. Following addition of resazurin/MHB buffer, the plate was immediately placed in a plate-reading fluorimeter for incubation overnight at either 37 °C (*E. coli*) or 30 °C (*B. cereus*) while monitoring fluorescence for each well (530 nm_{ex}/590 nm_{em}). These antimicrobial measurements were performed in triplicate in order to provide statistical significance.

Fluorescence data for each well was compiled and the onset time of half maximal fluorescence ($T_{0.5}$) was determined. For both *E. coli* and *B. cereus*, standard curves were generated using serially diluted bacterial suspensions (~10^6 CFU/mL–10^3 CFU/mL) in the absence of CAMPs. Observed $T_{0.5}$ values were plotted against initial CFU counts, which were verified by plating on MHB agar plates. Analysis of the data by linear regression produces the following Eq. (1) for *E. coli* and Eq. (2) for *B. cereus*.

$$\log(\mathrm{CFU/mL}_{E.\ coli}) = -0.0002(T_{0.5}) + 9.314 \quad (1)$$

$$\log(\mathrm{CFU/mL}_{B.\ cereus}) = -0.0002(T_{0.5}) + 6.475 \quad (2)$$

Eqs. (1) and (2) were then used to interpolate the surviving bacterial concentration (CFU/mL) based on $T_{0.5}$ values determined following incubation with varied peptide concentrations. These values were used to calculate bacterial survival (%) relative to cultures incubated in the absence of peptide. The peptide concentration required to kill 50% of the viable cells in the assay (EC50) was determined by plotting survival as a function of the log of peptide concentration (log mg/mL) and fitting the data, using GraphPad Prism X5 (Graph-Pad Software, San Diego, CA) to Eq. (3), which describes a sigmoidal dose–response curve.

$$Y = \mathrm{Bottom} + \left((\mathrm{Top} - \mathrm{Bottom})/\left(1 + 10^{[(\log EC50 - X) * \mathrm{Hill\ Slope}]}\right)\right) \quad (3)$$

2.3. Antimicrobial kinetics

The antimicrobial kinetics of NA-CATH, L-ATRA-1A and D-ATRA-1A were evaluated in triplicate under both low (10 mM phosphate buffer, pH 7.4) and high (10 mM phosphate buffer, 100 mM KCl, pH 7.4) salt conditions at peptide concentrations of 200, 2 and 0.2 μg/mL and time intervals of 0.5, 2, 4, 10 and 20 min. In a 96-well plate, 55 μL of a 400 μg/mL peptide solution in buffer was added to 5 wells (1 well for each time point) and then serially diluted by taking 5 μL of peptide into 50 μL of buffer. Frozen aliquots of either *E. coli* or *B. cereus* were thawed on ice and then diluted in buffer to a concentration of 1×10^5 CFU/mL. Using a multi-channel pipette, 50 μL of bacterial stock was added to each well containing peptide solution. Additionally, aliquots of bacterial stock were added to wells containing 50 μL of buffer as a survival reference. The prepared plate was allowed to incubate at room temperature with samples being collected at 0.5, 2, 4, 10 and 20 min. Samples collected for each time point were diluted 10-fold by taking 50 μL from the 96-well plate into 450 μL of 1× PBS and then serially diluted using the same buffer. The surviving bacteria were plated in triplicate and incubated for 18 h at 37 ° C (*E. coli*) or 30 ° C (*B. cereus*). The percentage of the bacterial killing relative to the control was determined for each peptide concentration at each time point. The percent killing for each peptide concentration was plotted as a function of time.

2.4. Membrane depolarization assay

Cytoplasmic membrane depolarization was determined using the membrane potential-sensitive cyanine dye $diSC_3$-(5). In this method, frozen aliquots of enumerated bacteria (*E. coli* or *B. cereus*) were thawed on ice and washed 3 times with buffer (5 mM HEPES with 20 mM glucose, pH 7.4). Following washing, the pelleted bacteria were re-suspended in HEPES buffer (5 mM HEPES, pH 7.4, 20 mM glucose) containing either, 10 or 100 mM KCl. A 96-well plate was prepared where wells are charged with 360 μL of bacterial suspension (2×10^7 CFU/mL) and 4.19 μL of $diSC_3$-(5) (200 nM) for a total volume of 364.19 μL. The bacteria were incubated at room temperature and fluorescence was monitored (622 nm_{ex}/670 nm_{em}) until $diSC_3$-(5) maximal uptake was obtained. Maximal $diSC_3$-(5) uptake is indicated by a baseline in fluorescence due to self-quenching as the dye concentrates in the cell membrane. Peptide (NA-CATH, L- or D-ATRA-1A) was added at varied concentrations (200–2 μg/mL) in 20 μL aliquots and the fluorescence increase due to induced depolarization of the cytoplasmic membrane was recorded. A negative control of bacteria and $diSC_3$-(5) was used as a background. As a positive control, complete collapse of the membrane potential was attained with valinomycin (200–2 μg/mL), a potassium ionophore. Measurements were performed in triplicate for each condition and each peptide. The peptide-induced fluorescence was baseline subtracted for each peptide and the maximal relative fluorescence units (RFU) were plotted as a function of peptide concentration.

2.5. SYTOX Green uptake assay

Induced membrane permeabilization caused by NA-CATH, L- or D-ATRA-1 was monitored via the fluorescence increase that occurs when the cationic cyanine dye SYTOX Green intercalates DNA. SYTOX Green is impermeant to living cells, yet can easily penetrate compromised membranes [4,20–22]. In this method, frozen aliquots of enumerated bacteria (*E. coli* or *B. cereus*) were thawed on ice and washed 3 times with buffer (5 mM HEPES with 20 mM glucose, pH 7.4). Following the final wash, the bacteria were pelleted and then re-suspended in 1 mL of HEPES buffer (5 mM HEPES with 20 mM glucose, pH 7.4) containing either 10 or 100 mM KCl. Aliquots of re-suspended bacteria were further diluted with their respective buffers to a concentration of 4×10^7 CFU/mL in 1 mL. The diluted cells were then charged with 1 μL of 5 mM SYTOX Green and incubated for 15 min in the dark at room temperature. Following incubation, bacteria-SYTOX suspension was added in 100 μL aliquots to the wells of a 96-well plate and the fluorescence of each well monitored in order to establish baseline fluorescence. After baseline fluorescence collection, 100 μL aliquots of peptide solutions, with concentrations ranging from 200 to 2 μg/mL, were added to each well and the increase in SYTOX Green fluorescence was measured (485 nm_{ex}/520 nm_{em}). As a negative control, fluorescence data was collected for bacteria suspended in buffer containing SYTOX Green in the absence of peptide. As a positive control, melittin (200–2 μg/mL) was added to bacterial cells to achieve complete lysis and maximum fluorescence. Measurements were performed in triplicate for each condition and each peptide. The peptide-induced fluorescence was baseline subtracted for each peptide and the maximal relative fluorescence units (RFU) were plotted as a function of peptide concentration.

2.6. Scanning electron microscopy

Enumerated frozen aliquots of either *E. coli* or *B. cereus* were thawed on ice and then diluted to a concentration of 2×10^8 CFU/mL using 10 mM phosphate buffer (pH 7.4). Stock solutions were prepared for NA-CATH, L-ATRA-1A and D-ATRA-1A (100 μg/mL) in 10 mM phosphate buffer (pH 7.4). Bacterial suspension and peptide solutions (50 μL each) were added to the wells of a 96-well plate giving a final

Table 1
Antimicrobial performance of NA-CATH and ATRA-1A isomers under high and low salt conditions. Antimicrobial activity is expressed in terms of EC50 (μg/mL) values with corresponding 95% confidence interval ranges for *E. coli* and *B. cereus*.
*Values were obtained using a plating assay and have been previously published [13].

Bacterium	Antimicrobial activity (EC50, μg/mL)											
	NA-CATH				L-ATRA-1A				D-ATRA-1A			
	High salt	95% CI range	Low salt	95% CI range	High salt	95% CI range	Low salt	95% CI range	High salt	95% CI range	Low salt	95% CI range
E. coli	0.024	0.015 to 0.040	0.023	0.022 to 0.025	~9.7	Very wide	4.3*	4.0 to 4.6	~7.1	Very wide	1.4*	1.1 to 1.5
B. cereus	0.60	0.49 to 0.72	0.35	0.33 to 0.40	N/A	N/A	73*	65 to 82	4.3	3.8 to 4.9	2.3*	2.1 to 2.6

peptide concentration of 50 μg/mL, which represents a mid-range peptide concentration based on those used in the membrane disruption assays. Controls consisting of bacteria alone suspended in buffer, as well as, peptide alone suspended in buffer were similarly prepared. Treated cells were then incubated for 20 min at room temperature. Following incubation, bacterial-peptide and control solutions were filtered on to a 0.22 μm membrane filter that had been pretreated with 0.1% poly-L-lysine in order to improve cell adhesion to the filter [23]. The retentates on the membrane surface were fixed for 2 h with 2.5% glutaraldehyde, dehydrated with graded ethanol series and then critical point dried. An 8 nm layer of Au/Pd alloy was sputtered on the samples to avoid charging in the microscope. Samples were imaged in high resolution mode with an upper detector using a Hitachi-4700[3] FESEM at an accelerating voltage of 10 keV.

3. Results and discussion

3.1. Antimicrobial effectiveness and kinetics

Ionic strength in media has historically been shown to impact the antimicrobial activity of CAMPs [24–27]. For many CAMPs, high salt conditions impede their ability to kill bacteria, however the degree to which the peptides are affected can vary significantly. Here, the antimicrobial properties and bactericidal kinetics of full-length NA-CATH and the ATRA-1A isomers have been assessed against representative Gram-negative and Gram-positive bacteria, *E. coli* and *B. cereus*, respectively under low and high salt conditions.

In order to assess the degree to which salt conditions impact their antimicrobial effectiveness, the performances of NA-CATH, L-ATRA-1A and D-ATRA-1A were evaluated against *E. coli* and *B. cereus* under both low (10 mM phosphate buffer, pH 7.4) and high (100 mM KCl in 10 mM phosphate buffer, pH 7.4) salt conditions. The results of these assays indicate that the half-maximal effective concentration (EC50) values for the peptides are dependent on both the nature of the bacteria being tested and the salt conditions (Table 1). Against the Gram-negative bacterium, *E. coli*, the EC50 values in low salt for NA-CATH, L-ATRA-1A and D-ATRA-1A were 0.023 μg/mL, 4.3 μg/mL and 1.4 μg/mL, respectively. In high salt conditions NA-CATH had an EC50 of 0.024 μg/mL, while L-ATRA-1A and D-ATRA-1A had EC50s of ~9.7 μg/mL and ~7.1 μg/mL, respectively. When tested against *B. cereus*, a Gram-positive bacterium, the EC50 values for low salt conditions were found to be 0.35 μg/mL, 73 μg/mL, and 2.3 μg/mL for NA-CATH, L-ATRA-1A and D-ATRA-1A, respectively. In high salt conditions, the EC50 value found for NA-CATH was 0.60 μg/mL and that of D-ATRA-1A was 4.3 μg/mL. L-ATRA-1A was completely ineffective against *B. cereus* under these conditions.

In addition to antimicrobial potency, the rate with which the peptides exerted their bactericidal effect was evaluated under both low and high salt conditions (*E. coli* — Fig. 2 and *B. cereus* — Fig. 3). Here, initial killing kinetics were established by monitoring bacterial survival as a function of time for the first 20 min following introduction of peptide to the bacterial culture. In these studies, three peptide concentrations were evaluated based on the range of EC50 values exhibited by the ATRA-1A isomers against *E. coli* and *B. cereus*; a sub EC50 concentration (0.2 μg/mL), a concentration near EC50 (2 μg/mL) and a supra EC50 concentration (200 μg/mL). Under low salt conditions, the peptides exhibited differences in their antimicrobial kinetics against both bacteria. At a concentration of 200 μg/mL, full-length NA-CATH achieved complete killing in less than 30 s against both *E. coli* (Fig. 2A) and *B. cereus* (Fig. 3A). After 20 min, NA-CATH displayed ~25% killing at a peptide concentration of 2 μg/mL and ~5% killing at 0.2 μg/mL for both *E. coli* (Fig. 2; B and C) and *B. cereus* (Fig. 3; B and C). Under the same conditions, L-ATRA-1A exhibited ~100% killing against *E. coli* at 200 μg/mL, while presenting ~25% killing at 2 μg/mL and ~20% killing at 0.2 μg/mL (Fig. 2; A–C) after 20 min. Against *B. cereus*, ~90% killing was observed for L-ATRA-1A at 200 μg/mL after 20 min, while ~20% killing was achieved at 2 μg/mL and ~10% killing at 0.2 μg/mL in the same timeframe (Fig. 3; A–C). While, D-ATRA-1A exhibited 100% killing at 200 μg/mL, ~50% killing at 2 μg/mL and ~20% killing at 0.2 μg/mL (Fig. 2; A–C) against *E. coli* after 20 min. Against *B. cereus*, D-ATRA-1A exhibited 100% and ~50% killing after 20 min at peptide concentrations of 200 μg/mL and 2 μg/mL, respectively (Fig. 3; A and B), however diminished killing (~5%) occurred at 0.2 μg/mL (Fig. 3C).

Under high salt conditions, the peptides exhibited changes in their killing kinetics against both *E. coli* (Fig. 2D–F) and *B. cereus* (Fig. 3D–F). However, NA-CATH at a concentration of 200 μg/mL kills 100% of bacteria within 30 s for both *E. coli* and *B. cereus*, which is consistent with the kinetics observed under low salt conditions (Figs. 2D and 3D). At lower concentrations, NA-CATH demonstrated ~45% killing after 20 min at a peptide concentration of 2 μg/mL and ~0% killing at 0.2 μg/mL of peptide for *E. coli* (Fig. 2E and F), and ~35% killing at 2 μg/mL of peptide and ~15% killing at 0.2 μg/mL for *B. cereus* (Fig. 3E and F). The killing kinetics for L-ATRA-1A against both *E. coli* and *B. cereus* were significantly reduced under high salt conditions relative to the killing kinetics observed in low salt medium. Against *E. coli*, L-ATRA-1A exhibited ~25%, ~20%, and ~10% killing after 20 min at peptide concentrations of 200 μg/mL, 2 μg/mL and 0.2 μg/mL, respectively (Fig. 2D–F). After 20 min incubation with *B. cereus*, L-ATRA-1A showed killing of ~25% at 200 μg/mL of peptide, ~15% at 2 μg/mL and ~0% at 0.2 μg/mL (Fig. 3D–F). Against *E. coli*, D-ATRA-1A exhibited slower killing kinetics in high salt relative to that observed in low salt conditions. Incubation of D-ATRA-1A with *E. coli* for 20 min resulted in killing of ~25%, ~25% and ~0% at peptide concentrations of 200 μg/mL, 2 μg/mL and 0.2 μg/mL, respectively (Fig. 2D–F). Against *B. cereus*, D-ATRA-1A showed ~25% killing at concentrations of 200 μg/mL and 2 μg/mL, while at 0.2 μg/mL exhibited ~10% killing (Fig. 3D–F). From this data it is clear that the salt conditions impact the killing kinetics of NA-CATH and the ATRA-1A isomers, however the extent of the effect appears to vary depending on the peptide and the bacterial strain.

The kinetics of antibacterial effectiveness, illustrated in Figs. 2 and 3, have been observed for only the initial 20 min following addition of peptide. The data indicates that NA-CATH's mechanism of action, at peptide concentrations near the EC50, requires incubation for longer than 20 min in order to exert its full bactericidal effectiveness. Against *E. coli*, NA-CATH was unable to achieve 50% killing at peptide concentrations of 0.2 and 2 μg/mL within the 20 minute window, which are 10 and 100 times its EC50 determined in both low and high salt conditions

[3] Commercial equipment and material suppliers are identified in this paper to adequately describe experimental procedures. This does not imply endorsement by NIST.

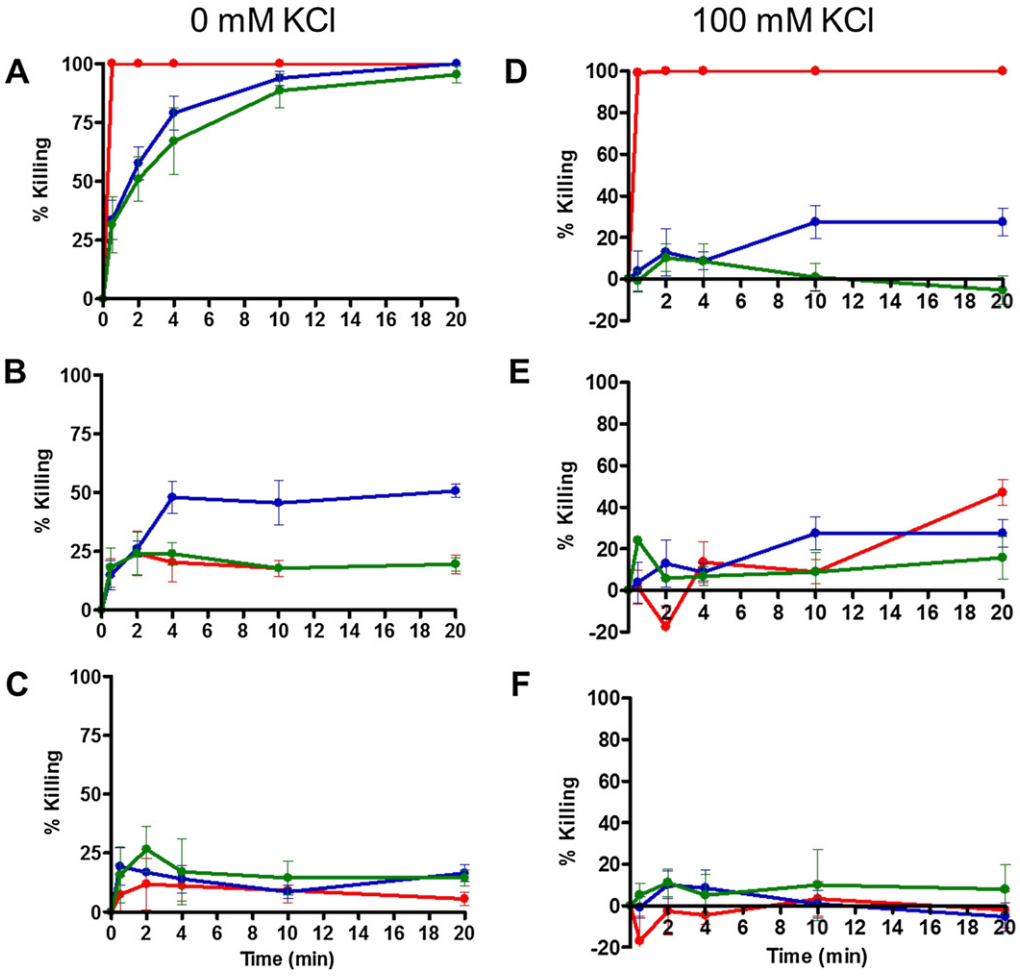

Fig. 2. Antimicrobial kinetics of NA-CATH and the ATRA-1A isomers against *E. coli*. The killing kinetics of NA-CATH (red), L-ATRA-1A (green) and D-ATRA-1A (blue) were evaluated against *E. coli* in low salt conditions and high salt conditions at peptide concentrations of 200 μg/mL (A and D), 2 μg/mL (B and E) and 0.2 μg/mL (C and F). The data are reported as the average of n = 3 and the 95% confidence interval (CI) is indicated where appropriate.

(0.023 μg/mL and 0.024 μg/mL, respectively). Similar results were exhibited by NA-CATH against the Gram-positive bacterium *B. cereus*, where half-maximal effectiveness was not achieved within the 20 minute time frame at a peptide concentration of 2 μg/mL, which is ~6 times the EC50 in low salt conditions (0.35 μg/mL) and ~ 3 times the EC50 value in high salt (0.60 μg/mL). Interestingly, at a supra EC50 peptide concentration of 200 μg/mL, NA-CATH was able to completely kill 100% of both bacterial strains within 30 s regardless of salt conditions.

The killing kinetics of L-ATRA-1A against *E. coli* under low-salt conditions showed a quarter of the population surviving after 20 min of incubation with 2 μg/mL of peptide, which is half the EC50 value (4.3 μg/mL). While at a peptide concentration of 200 μg/mL (~46 times its EC50 value), L-ATRA-1A achieved nearly 100% killing after 20 min. In high salt conditions, L-ATRA-1A failed to attain 50% killing against *E. coli* within the 20 minute window even at a peptide concentration of 200 μg/mL, which is 20 times its EC50 (9.7 μg/mL). In low salt conditions, L-ATRA-1A only reaches above 50% killing of *B. cereus* in the same time period at a peptide concentration of 200 μg/mL, which is ~3 times its EC50 value (73 μg/mL). This peptide exhibited limited killing against *B. cereus* in high salt conditions, even at a peptide concentration of 200 μg/mL, which is consistent with the lack of killing observed in the antimicrobial assays performed under similar conditions (no measurable EC50). In contrast, the killing kinetics of D-ATRA-1A showed 50% killing against *E. coli* at a peptide concentration of 2 μg/mL under low salt conditions within 20 min, which is similar to the peptides EC50 in the same conditions (1.4 μg/mL). Complete killing was obtained at a D-ATRA-1A concentration of 200 μg/mL for *E. coli* in low salt conditions. Against *B. cereus*, D-ATRA-1A exhibited similar results in low salt conditions with 50% killing being achieved at a peptide concentration of 2 μg/mL, which is approximately equal to its EC50 value of 2.3 μg/mL. As was the case with *E. coli*, 100% killing was obtained against *B. cereus* using D-ATRA-1A at a peptide concentration of 200 μg/mL under low salt conditions. While the D-peptide failed to attain 50% killing against either bacterial strain in high salt conditions in the observed 20 minute window, even at a peptide concentration of 200 μg/mL, which is 28 times its EC50 against *E. coli* (7.1 μg/mL) and 50 times its EC50 against *B. cereus* (4.3 μg/mL).

The observed decreases in killing activity for the peptides in high salt conditions are likely the result of multiple contributing factors. Direct interaction of salt ions with the peptide's hydrophilic residues and the lipid-bilayer head groups shields their respective charges and reduces the electrostatic interactions [26]. Additionally, the high levels of activity observed for the peptides under low salt (0 KCl) conditions may reflect increased bacterial susceptibility to membrane disruption and lysis in such hypotonic environments [28]. Hofmeister effects, ionic screening and specific ion binding between the solution ions and both peptide side-chains and lipid head groups all likely contribute to the observed reductions in antimicrobial effectiveness [29–32]. For example, these interactions could result in a reduction in CAMP helicity, and thus amphipathic character, which would greatly affect their ability to directly interact with bacterial membranes and reduce or negate their antimicrobial effectiveness.

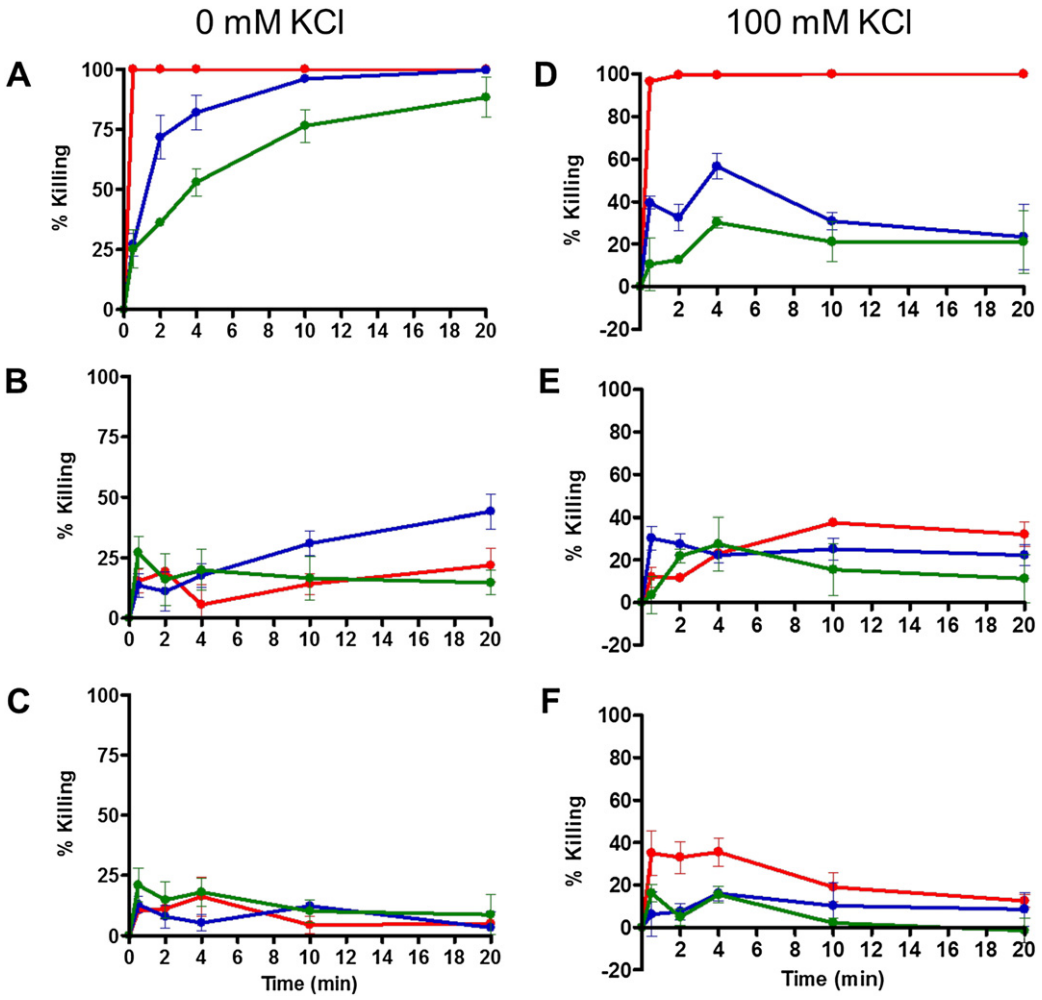

Fig. 3. Antimicrobial kinetics of NA-CATH and the ATRA-1A isomers against *B. cereus*. The killing kinetics of NA-CATH (red), L-ATRA-1A (green) and D-ATRA-1A (blue) were evaluated against *B. cereus* in low salt conditions and high salt conditions at peptide concentrations of 200 μg/mL (A and D), 2 μg/mL (B and E) and 0.2 μg/mL (C and F). The data are reported as the average of n = 3 and the 95% confidence interval (CI) is indicated where appropriate.

3.2. Bacterial membrane disruption

Cationic antimicrobial peptides in general have been shown to be capable of causing varying degrees of disruption in bacterial membranes, ranging from transient gaps, to large pores and micellization. Accordingly, the extent to which NA-CATH and the ATRA-1A isomers interact with bacterial membranes was ascertained using assays designed to monitor membrane depolarization and permeabilization over a range of peptide concentrations (2, 12.5, 25, 50, 100 and 200 μg/mL). Depolarization of bacterial membranes was evaluated using $diSC_3$-(5), a membrane potential sensitive dye, which concentrates within the lipid bilayer resulting in the dye self-quenching [4,22,27,33,34]. If peptides depolarize the membrane, the potential dissipates, and $diSC_3$-(5) is released into solution causing an increase in fluorescence, which is directly proportional to the degree of membrane potential reduction. Uptake of SYTOX Green, a nucleic acid stain, was used to detect greater degrees of peptide-induced membrane permeabilization. SYTOX Green is impermeant to the membranes of healthy cells, but can penetrate disrupted cell membranes and bind to nucleic acids [21]. If the bacterial cell membrane integrity is compromised by pores large enough to allow passage or cell lysis, influx of the dye and subsequent binding to DNA causes a >500-fold increase in fluorescence [4,20–22]. Scanning electron microscopy (SEM) allows for visualization of morphological changes in bacterial membranes [20,35–37]. Therefore, SEM was used to probe the ability of the CAMPs to induce gross changes in membrane morphology, including blebbing, aggregation, pore formation and cell lysis.

The results of the $diSC_3$-(5) depolarization studies indicate that all three peptides differentially dissipate membrane potential in *E. coli* and *B. cereus* to varying degrees, depending on peptide concentration and salt conditions. In low salt conditions, NA-CATH was able to depolarize both *E. coli* (Fig. 4A) and *B. cereus* (Fig. 4B) cells at 2 μg/mL, the lowest peptide concentration tested, with depolarization increasing as the peptide concentration increased. Under high salt conditions, NA-CATH induced depolarization was not detected against *E. coli* cells at peptide concentrations below 100 μg/mL, with depolarization at 100 and 200 μg/mL being considerably lower than those seen in low salt conditions (Fig. 4C). In contrast, NA-CATH caused depolarization of *B. cereus* cells at a peptide concentration of 2 μg/mL under high salt conditions, with depolarization increasing as the peptide concentration increased up to 100 μg/mL (Fig. 4D). However, increasing the peptide concentration from 100 μg/mL to 200 μg/mL resulted in no significant change in depolarization. Under low salt conditions, both L- and D-ATRA-1A exhibited depolarization of *E. coli* cells at peptide concentrations as low as 2 μg/mL, with increased depolarization occurring at higher peptide concentrations (Fig. 4A). On the other hand, the ATRA-1A isomers only produced slight depolarization of *B. cereus* at peptide concentrations ranging from 12.5 μg/mL to 200 μg/mL (Fig. 4B). In high salt conditions, L-ATRA-1A exhibited no depolarization against *E. coli* (Fig. 4C) and very little depolarization against *B. cereus*, even at

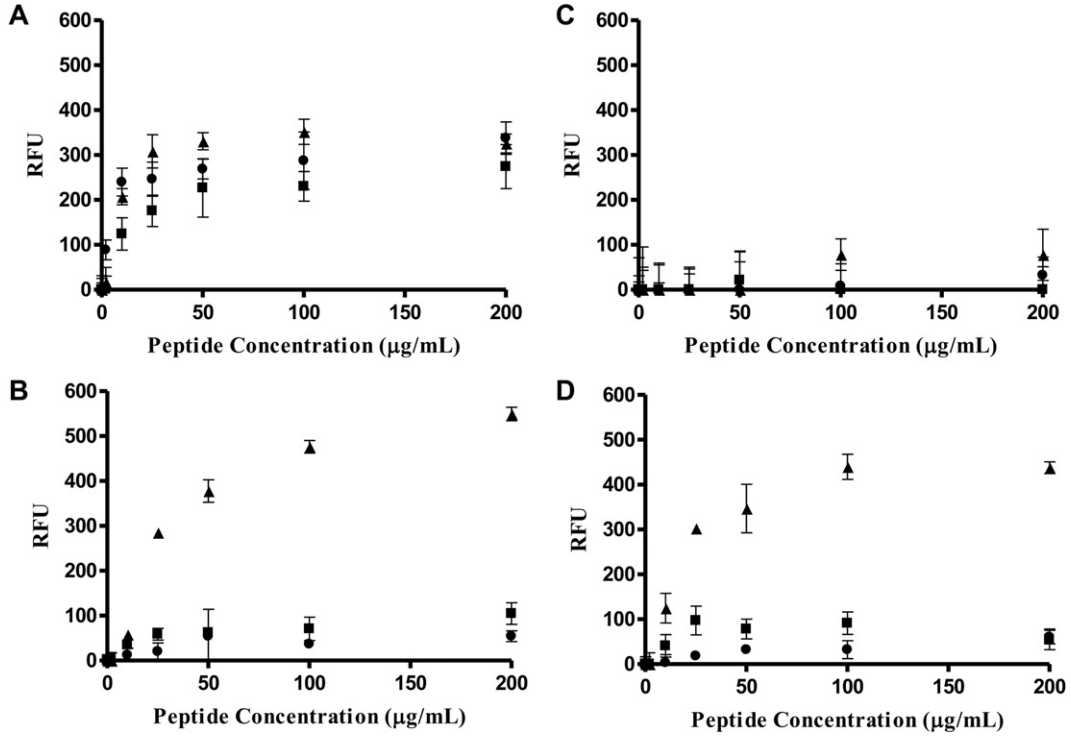

Fig. 4. Effect of peptide concentration on membrane depolarization. Using $diSC_3$-(5) fluorescence to monitor the effect of peptide concentration on induced membrane depolarization for NA-CATH (▲), L-ATRA-1A (●) and D-ATRA-1A (■) in low salt conditions against *E. coli* (A) and *B. cereus* (B) and high salt conditions *E. coli* (C) and *B. cereus* (D). The data are reported as the average of n = 3 and the standard deviation is indicated by the error bars.

the highest peptide concentrations tested (Fig. 4D). Similarly, treatment of *E. coli* with D-ATRA-1A in high salt conditions did not afford significant depolarization (Fig. 4C). However, D-ATRA-1A induced slightly greater depolarization against *B. cereus* than was achieved using L-ATRA-1A (Fig. 4D).

From these results, it is evident that all three peptides exhibited higher degrees of depolarization in a low salt environment than under high salt conditions. In low salt conditions, L-ATRA-1A and D-ATRA-1A displayed higher degrees of depolarization with *E. coli* than with *B. cereus*, while NA-CATH showed similar depolarization with both bacterial strains. Under high salt conditions, all three peptides showed depolarization of *B. cereus*, while only NA-CATH exhibited any significant depolarization with *E. coli*. Membrane depolarization data for the three peptides is consistent with their antimicrobial effectiveness and killing kinetics.

To further investigate the extent of membrane disruption induced by NA-CATH and the ATRA-1A isomers, SYTOX Green fluorescence was used as a reporter to assess membrane permeabilization and the formation of larger pores and openings in bacterial membranes. In these studies, none of the peptides exhibited significant membrane permeabilization against *E. coli* under either low or high salt conditions (Fig. 5A and C). However, NA-CATH was able to permeabilize the membranes of *B. cereus* under both salt conditions at peptide concentrations as low as 25 μg/mL (Fig. 5B and D). Neither L-ATRA-1A nor D-ATRA-1A was able to permeabilize the membranes of *B. cereus* in either low or high salt conditions (Fig. 5A–D).

In the SYTOX Green uptake studies, NA-CATH induced membrane disruption in Gram-positive bacterium *B. cereus* in both high and low salt environments, which is consistent with the peptide's performance in $diSC_3$-(5) depolarization studies. Against the Gram-negative bacterium *E. coli*, NA-CATH was unable to permeabilize the bacterial membrane in either high or low salt conditions. This is in contrast to the performance of NA-CATH in $diSC_3$-(5) assays, where the peptide was able to induce membrane depolarization in *E. coli* under low salt conditions. In the cases of L-ATRA-1A and D-ATRA-1A, no SYTOX fluorescence was displayed, even under low salt conditions where these peptides exhibited significant depolarization.

Greater understanding of the ability of CAMPs to inflict gross changes in bacterial membranes can be achieved using SEM to visualize morphological changes in bacteria that have been treated with either NA-CATH or one of the ATRA-1A isomers. The exposure of *E. coli* and *B. cereus* to 50 μg/mL of peptide for 20 min resulted in notable alterations in cell morphology. When untreated *E. coli* cells were prepared from low ionic strength buffer, the SEM images showed intact cells with a corrugated morphology, typical of this strain (Fig. 6I; A and B) [35]. However, *E. coli* exposed to peptide presented multiple structural abnormalities. After incubation with L-ATRA-1A, the appearance of the *E. coli* cells changed drastically, displaying blebbing on the cell surface with some exhibiting cellular leakage (Fig. 6I; C and D). Similar alterations were seen in *E. coli* treated with D-ATRA-1A, however the extent of surface blebbing was significantly greater (Fig. 6I; E and F). *E. coli* exposed to NA-CATH exhibited large blebs along their surface, cellular leakage, as well as cell lysis (Fig. 6I; G and H). Untreated *B. cereus* prepared from low ionic strength buffer in the absence of peptide appeared normal, exhibiting smooth cell membranes and minimal aggregation (Fig. 7I, A and B). Minor morphological changes were observed in *B. cereus* exposed to L-ATRA-1A, which displayed roughening of the cell surface and micro-blebbing. Additionally, these cells exhibit increased regions of cellular aggregation (Fig. 7I; C and D). Treatment of *B. cereus* with D-ATRA-1A resulted in aggregation throughout the entire sample, as well as, membrane roughening and micro-blebbing (Fig. 7I; E and F). *B. cereus* cells treated with NA-CATH exhibited the highest degree of aggregation, along with membrane blebbing, cellular leakage, and large pore formation leading to cell lysis (Fig. 7I; G and H).

Under high salt conditions, the peptide-induced morphological alterations in both *E. coli* (Fig. 6 II) and *B. cereus* (Fig. 7 II) were muted relative to those produced in low salt conditions. When untreated *E. coli* were prepared from high ionic strength buffer, the SEM images showed intact cells with smoother surfaces than were seen in cells from low salt buffer (Fig. 6II; A and B). Incubation of *E. coli* with either

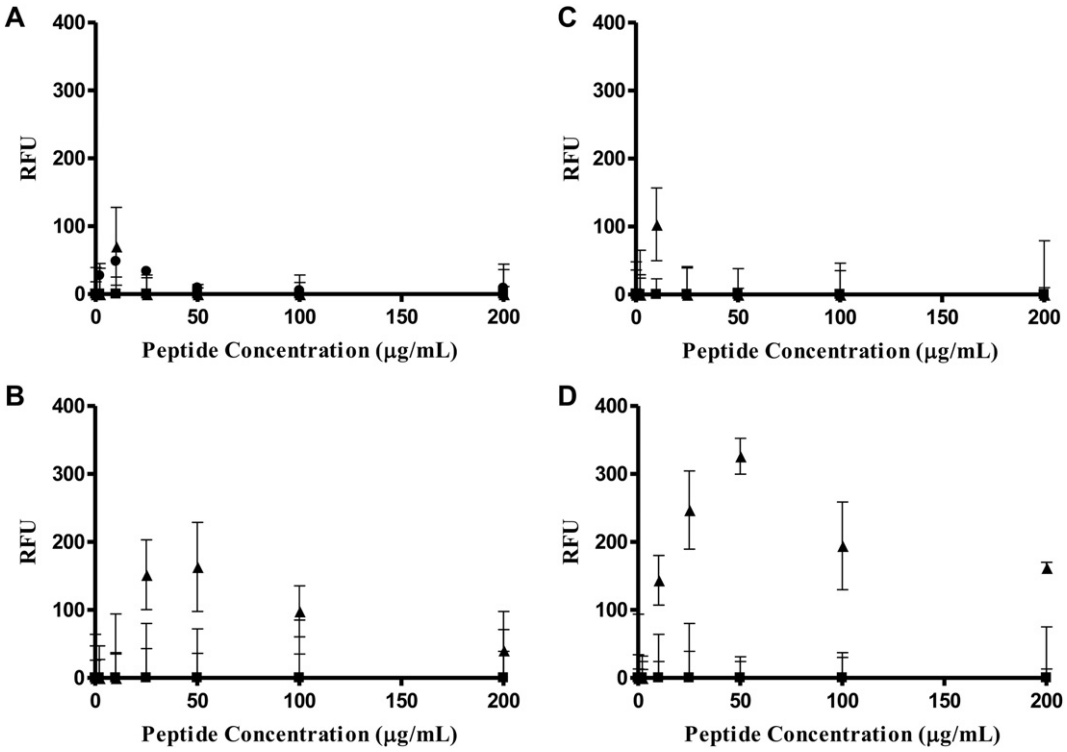

Fig. 5. Effect of peptide concentration on membrane permeabilization. Evaluation of peptide-induced membrane permeabilization based on SYTOX Green fluorescence using varied concentrations of NA-CATH (▲), L-ATRA-1A (●) and D-ATRA-1A (■) in low salt conditions against *E. coli* (A) and *B. cereus* (B) and high salt conditions *E. coli* (C) and *B. cereus* (D). The data are reported as the average of n = 3 and the standard deviation is indicated by the error bars.

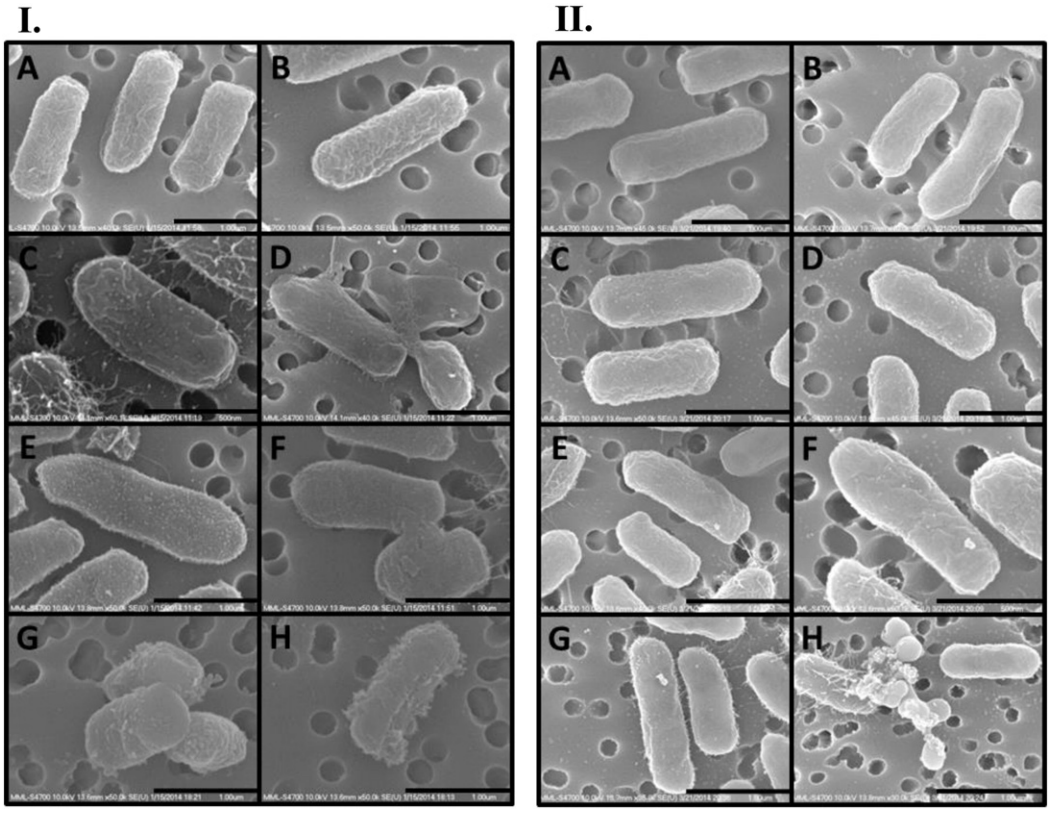

Fig. 6. SEM micrographs of *E. coli* following peptide exposure. I. *E. coli* untreated under low-salt conditions (A and B), and following incubation with L-ATRA-1A (C and D), D-ATRA-1A (E and F) and NA-CATH (G and H). In I A–H the scale bar is equal to 1 μm. II. *E. coli* untreated under high-salt conditions (A and B), and following incubation with L-ATRA-1A (C and D), D-ATRA-1A (E and F) and NA-CATH (G and H). In II A–H the scale bar is equal to 1 μm. While the selected images illustrate morphological changes observed in the samples, they do not reflect the distribution of these changes in the sample population.

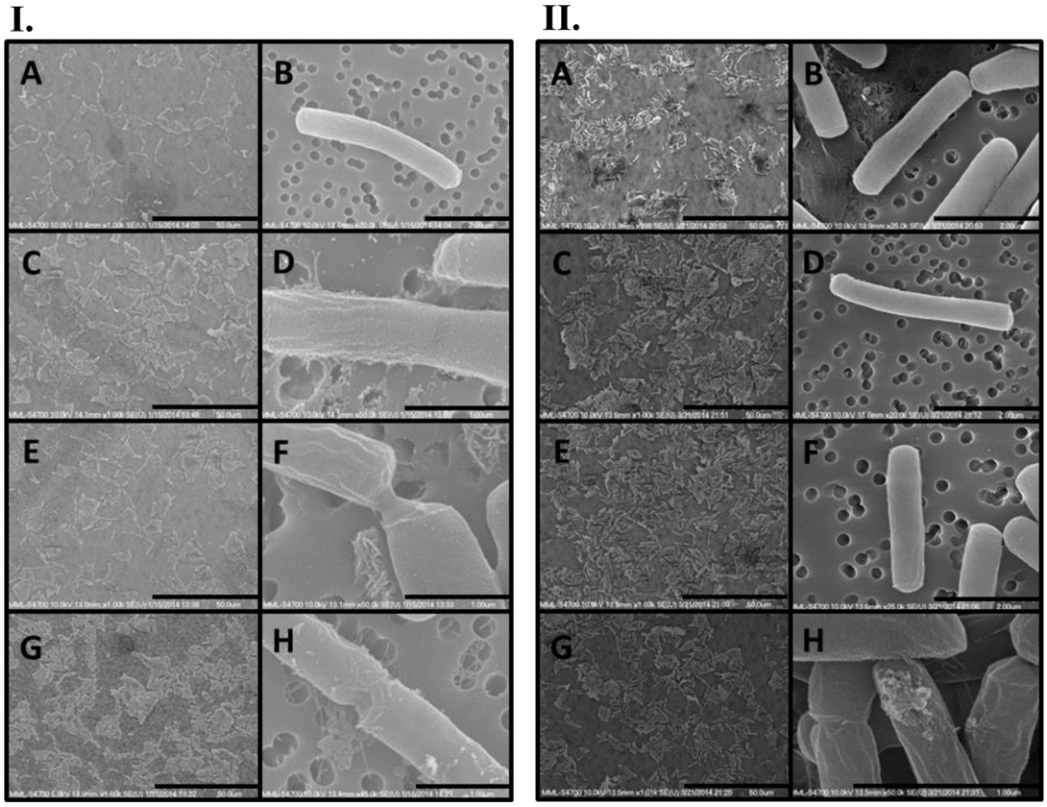

Fig. 7. SEM micrographs of *B. cereus* following peptide exposure. I. *B. cereus* untreated under low-salt conditions (A and B), and following incubation with L-ATRA-1A (C and D), D-ATRA-1A (E and F) and NA-CATH (G and H). In I the scale bar is equal to 50 μm (A, C, E, and G), 2 μm (B) and 1 μm (D, F, and H). II. *B. cereus* untreated under high-salt conditions (A and B), and following incubation with L-ATRA-1A (C and D), D-ATRA-1A (E and F) and NA-CATH (G and H). In II the scale bar is equal to 50 μm (A, C, E, and G) and 2 μm (B, D, F, and H). While the selected images illustrate morphological changes observed in the samples, they do not reflect the distribution of these changes in the sample population.

L-ATRA-1A or D-ATRA-1A afforded cells displaying similar degrees of surface roughening and membrane blebbing, however the level of blebbing was lower than that observed in similarly treated cells in low salt conditions (Fig. 6II; C, D, E and F). In high salt conditions, *E. coli* exposed to NA-CATH still exhibited substantial blebbing along their surface, cellular leakage, and cell lysis (Fig. 6II; G and H). Untreated *B. cereus* prepared in high salt displayed smooth cell morphology and increased aggregation relative to that seen in cells from low salt buffer (Fig. 7II, A and B). No changes in membrane morphology were observed in *B. cereus* exposed to L-ATRA-1A or D-ATRA-1A, however these cells did exhibit increased aggregation (Fig. 7II; C, D, E and F). Treatment of *B. cereus* with NA-CATH under high salt conditions resulted in cellular aggregation, as well as, roughening and micro-blebbing along the cell surface and incidences of cell lysis (Fig. 7II; G and H).

While the selected images illustrate the morphological changes that NA-CATH and the ATRA-1A isomers can inflict on bacterial membranes, scanning the entire sample provided a clearer impression of the distribution and extent of these changes within the bulk population. For both *E. coli* and *B. cereus*, the morphological changes caused by NA-CATH, in both low and high salt conditions, were more severe than those seen with either of the ATRA-1A isomers. The ATRA-1A isomers appeared to have a uniform effect across the entire bacterial populations for both *E. coli* and *B. cereus*. However, NA-CATH was less consistent in its affect, with some cells manifesting severe detrimental morphological changes and others appearing less affected. At 13.6 mm × 35–20 k magnification, 2 out of 5 *E. coli* cells and 2 out of 6 *B. cereus* cells treated with NA-CATH under low salt conditions exhibited visible damage to the bacterial membrane. While under high salt conditions, 1 out of 5 *E. coli* cells and 1 out of 7 *B. cereus* cells treated with NA-CATH demonstrated visible bacterial membrane damage at the same magnification.

The results of the membrane perturbation experiments employing $diSC_3$-(5) and SYTOX Green reflect bulk properties and do not distinguish the effect the peptides have on individual cells. By contrast, SEM allows examination of individual cells within the population, thus providing essential insights into the way that these peptides interact with membranes and the antimicrobial mechanisms that they employ. When the performance of NA-CATH and the ATRA-1A isomers in spectrophotometric assays is considered in conjunction with analysis of their respective SEM images, patterns begin to emerge suggesting both similarities and differences in the interactions of the peptides with bacterial membranes (Table 2). While L-ATRA-1A showed significant depolarization for *E. coli* in low salt conditions and moderate depolarization of *B. cereus* in both low and high salt environments, it did not exhibit permeabilization for either bacterial strain in SYTOX Green-based assays regardless of salt conditions. The SEM data for cells treated with L-ATRA-1A showed mainly roughening and blebbing of the cell membranes, suggesting that these membrane morphological changes are not indicative of permeabilization. Similarly, the spectrophotometric experiments showed that D-ATRA-1A produced strong depolarization of *E. coli* in low salt buffer and moderate depolarization of *B. cereus* in both low and high salt conditions, but failed to induce permeabilization in either bacterial strain under both salt conditions. However, SEM revealed that D-ATRA-1A produced a greater degree of blebbing than was observed in cells treated with L-ATRA-1A. While NA-CATH exhibited strong depolarization of *E. coli* and *B. cereus* and significant permeabilization of only *B. cereus* in the $diSC_3$-(5) and SYTOX Green assays, the SEM data revealed that the peptide had a more dramatic but less consistent impact on the cell morphology of both bacterial strains than was seen with the shorter ATRA-1A isomers. Despite their demonstrated ability to disrupt bacterial membrane integrity, none of the peptides exhibit significant hemolytic activity (see Supplemental material). This is significant because hemolytic assays are frequently used to evaluate the propensity of CAMPs to attack host cell membranes.

Table 2
Qualitative comparison of spectrophotometric assay results and SEM image analysis. The results from $diSC_3$-(5) and SYTOX Green assays and analysis of scanning electron microscopy images for *E. coli* (A) and *B. cereus* (B) treated with NA-CATH and the ATRA-1A isomers are illustrated in order to more effectively capture the difference in the performance of the peptides. Boxes shaded in white correspond to negative or slight response (−), light gray corresponds to a positive response (+) and dark gray corresponds to a strong positive response (++).

A

Peptide	E. coli									
	Spectrophotometric analysis				Scanning electron microscopy image analysis					
	Depolarization		Permeabilization		Aggregation		Blebbing		Lysis	
	High salt	Low salt	High salt	Low salt	High salt	Low salt	High salt	Low salt	High salt	Low salt
L–ATRA–1A	–	++	–	–	–	–	+	+	–	+
D–ATRA–1A	–	++	–	–	–	–	+	++	–	+
NA–CATH	+	++	–	–	–	–	++	++	+	++

B

Peptide	B. Cereus									
	Spectrophotometric analysis				Scanning electron microscopy image analysis					
	Depolarization		Permeabilization		Aggregation		Blebbing		Lysis	
	High salt	Low salt	High salt	Low salt	High salt	Low salt	High salt	Low salt	High salt	Low salt
L–ATRA–1A	+	+	–	–	++	++	–	+	–	–
D–ATRA–1A	+	+	–	–	++	++	–	+	–	–
NA–CATH	++	++	++	+	++	++	+	++	+	+

4. Conclusion

While detailed mechanisms of action for NA-CATH and the ATRA-1A peptides cannot be extracted solely from the data reported here, this research does provide insights into the potential avenues by which these peptides exert their antimicrobial effects and suggests that significant differences exist in the ways that each peptide interacts with bacterial membranes. In these studies, NA-CATH exhibits very high potency in both high and low salt environments and the ability to rapidly cause bacterial membrane disruption at low peptide concentrations. In the cases of the shorter ATRA-1A isomers, D-ATRA-1A appears to be more potent than its L-counterpart, however the data presented here suggests that the nature of their interactions with bacterial membranes is similar. SEM images for bacteria incubated with full-length NA-CATH reveal an uneven field of cell destruction, with some cells being completely lysed while others appear unaffected. In contrast, images for the ATRA-1A isomers exhibit more uniform but more modest disruption of bacterial membrane surfaces. These results are consistent with our earlier observation that exposure to high concentrations NA-CATH resulted in the complete lysis of anionic liposomes, while incubation with the ATRA-1A peptides appeared to cause liposome leakage, fusion and aggregation [15]. The current studies suggest NA-CATH and the ATRA-1A peptide isomers employ different mechanisms of action. The performance data and SEM images for NA-CATH appear to be consistent with membrane disruption mechanisms that involve a degree of cooperativity. The disruption mechanisms employed by the ATRA-1A isomers seem to be less cooperative, possibly involving modes of action resembling a carpet model. The differences observed in the behaviors of the full-length parent peptide, NA-CATH, and the truncated ATRA-1A isomers demonstrate how altering the length and charge of an antimicrobial peptide can impact not only their antimicrobial effectiveness, but can also dramatically affect the mechanism of action that they employ. Such mechanistic factors must be considered in future efforts to identify minimal antimicrobial units within larger naturally occurring peptides as the antimicrobial mechanisms that they employ may differ significantly from that of the parent peptide.

Conflict of interest statement

We have no conflict of interest.

Acknowledgements

We gratefully acknowledge DTRA HDTRA1-12-C-0039 and the GMU College of Science for support.

Appendix A. Supplementary data

Supplementary data to this article can be found online at http://dx.doi.org/10.1016/j.bbamem.2015.01.007.

References

[1] R.E. Hancock, M.G. Scott, The role of antimicrobial peptides in animal defenses, Proc. Natl. Acad. Sci. U. S. A. 97 (2000) 8856–8861.
[2] Y. Shai, Mode of action of membrane active antimicrobial peptides, Biopolym. Pept. Sci. 66 (2002) 236–248.
[3] K.A. Brogden, Antimicrobial peptides: pore formers or metabolic inhibitors in bacteria? Nat. Rev. Microbiol. 3 (2005) 238–250.
[4] R. Rathinakumar, W.F. Walkenhorst, W.C. Wimley, Broad-spectrum antimicrobial peptides by rational combinatorial design and high-throughput screening: the importance of interfacial activity, J. Am. Chem. Soc. 131 (2009) 7609–7617.
[5] V. Teixeira, M.J. Feio, M. Bastos, Role of lipids in the interaction of antimicrobial peptides with membranes, Prog. Lipid Res. 51 (2012) 149–177.
[6] M. Yeaman, N. Yount, Mechanisms of antimicrobial peptide action and resistance, Pharmacol. Rev. 55 (2003) 27–55.
[7] D. Sengupta, H. Leontiadou, A.E. Mark, S.J. Marrink, Toroidal pores formed by antimicrobial peptides show significant disorder, Biochim. Biophys. Acta Biomembr. 1778 (2008) 2308–2317.
[8] E. Kosciuczuk, P. Lisowski, J. Jarczak, N. Strzałkowska, A. Jozwik, J. Horbanczuk, J. Krzyzewski, L. Zwierzchowski, E. Bagnicka, Cathelicidins: family of antimicrobial peptides. A review, Mol. Biol. Rep. 1–14 (2012).
[9] L. Tomasinsig, M. Zanetti, The cathelicidins—structure, function and evolution, Curr. Protein Pept. Sci. 6 (2005) 23–34.
[10] R. Bals, J.M. Wilson, Cathelicidins—a family of multifunctional antimicrobial peptides, Cell. Mol. Life Sci. 60 (2003) 711–720.
[11] M. Zanetti, Cathelicidins, multifunctional peptides of the innate immunity, J. Leukoc. Biol. 75 (2004) 39–48.

[12] Y. Wang, J. Hong, X. Liu, H. Yang, R. Liu, J. Wu, A. Wang, D. Lin, R. Lai, Snake cathelicidin from *Bungarus fasciatus* is a potent peptide antibiotics, PLoS ONE 3 (2008) 9.
[13] H. Zhao, T.-X. Gan, X.-D. Liu, Y. Jin, W.-H. Lee, J.-H. Shen, Y. Zhang, Identification and characterization of novel reptile cathelicidins from elapid snakes, Peptides 29 (2008) 1685–1691.
[14] F.A. De Latour, L.S. Amer, E.A. Papanstasiou, B.M. Bishop, M.L. Van Hoek, Antimicrobial activity of the *Naja atra* cathelicidin and related small peptides, Biochem. Biophys. Res. Commun. 396 (2010) 825–830.
[15] M. Juba, D. Porter, S. Dean, S. Gillmor, B. Bishop, Characterization and performance of short cationic antimicrobial peptide isomers, Biopolymers 100 (2013) 387–401.
[16] D. Wade, A. Boman, B. Wåhlin, C.M. Drain, D. Andreu, H.G. Boman, R.B. Merrifield, All-D amino acid-containing channel-forming antibiotic peptides, Proc. Natl. Acad. Sci. U. S. A. 87 (1990) 4761–4765.
[17] S.N. Dean, B.M. Bishop, M.L. van Hoek, Susceptibility of *Pseudomonas aeruginosa* biofilm to alpha-helical peptides: D-enantiomer of LL-37, Front. Microbiol. 2 (2011) 128.
[18] M.U. Shiloh, J. Ruan, C. Nathan, Evaluation of bacterial survival and phagocyte function with a fluorescence-based microplate assay, Infect. Immun. 65 (1997) 3193–3198.
[19] A. Mariscal, R.M. Lopez-Gigosos, M. Carnero-Varo, J. Fernandez-Crehuet, Fluorescent assay based on resazurin for detection of activity of disinfectants against bacterial biofilm, Appl. Microbiol. Biotechnol. 82 (2009) 773–783.
[20] M.L. Mangoni, N. Papo, D. Barra, M. Simmaco, A. Bozzi, A. Di Giulio, A.C. Rinaldi, Effects of the antimicrobial peptide temporin L on cell morphology, membrane permeability and viability of *Escherichia coli*, Biochem. J. 380 (2004) 859–865.
[21] B.L. Roth, M. Poot, S.T. Yue, P.J. Millard, Bacterial viability and antibiotic susceptibility testing with SYTOX green nucleic acid stain, Appl. Environ. Microbiol. 63 (1997) 2421–2431.
[22] J.Y. Kim, S.C. Park, J.K. Lee, S.J. Choi, K.S. Hahm, Y. Park, Novel antibacterial activity of β2-microglobulin in human amniotic fluid, PLoS ONE 7 (2012).
[23] M. Kalab, A. Yang, D. Chabot, Infocus Mag, Conventional scanning electron microscopy of bacteria, Infocus Mag. 10 (2008) 42–61.
[24] D.M.E. Bowdish, D.J. Davidson, Y.E. Lau, K. Lee, M.G. Scott, R.E.W. Hancock, Impact of LL-37 on anti-infective immunity, J. Leukoc. Biol. 77 (2005) 451–459.
[25] M.J. Goldman, G.M. Anderson, E.D. Stolzenberg, U.P. Kari, M. Zasloff, J.M. Wilson, Human beta-defensin-1 is a salt-sensitive antibiotic in lung that is inactivated in cystic fibrosis, Cell 88 (1997) 553–560.
[26] J.P. Tam, Y.-A. Lu, J.-L. Yang, Correlations of cationic charges with salt sensitivity and microbial specificity of cystine-stabilized beta-strand antimicrobial peptides, J. Biol. Chem. 277 (2002) 50450–50456.
[27] M. Wu, E. Maier, R. Benz, R.E. Hancock, Mechanism of interaction of different classes of cationic antimicrobial peptides with planar bilayers and with the cytoplasmic membrane of *Escherichia coli*, Biochemistry 38 (1999) 7235–7242.
[28] T.P.T. Cushnie, P.K.J. Robertson, S. Officer, P.M. Pollard, C. McCullagh, J.M.C. Robertson, Variables to be considered when assessing the photocatalytic destruction of bacterial pathogens, Chemosphere 74 (2009) 1374–1378.
[29] K. Xiong, E.K. Asciutto, J.D. Madura, S.A. Asher, Salt dependence of an alpha-helical peptide folding energy landscapes, Biochemistry 48 (2009) 10818–10826.
[30] J.S. Smith, J.M. Scholtz, Energetics of polar side-chain interactions in helical peptides: salt effects on ion pairs and hydrogen bonds, Biochemistry 37 (1998) 33–40.
[31] B.V. Sweet, A.K. Schwemm, D.M. Parsons, Review of the processes for FDA oversight of drugs, medical devices, and combination products, J. Manag. Care Pharm. 17 (2011) 40–50.
[32] C. Friedrich, M.G. Scott, N. Karunaratne, R.E.W. Hancock, Salt-resistant alpha-helical cationic antimicrobial peptides, Antimicrob. Agents Chemother. 43 (1999) 1542–1548.
[33] P.J. Sims, A.S. Waggoner, C.H. Wang, J.F. Hoffman, Studies on the mechanism by which cyanine dyes measure membrane potential in red blood cells and phosphatidylcholine vesicles, Biochemistry 13 (1974) 3315–3330.
[34] Y. Wang, Z. Zhou, J. Zhu, Y. Tang, T. Canady, Dark antimicrobial mechanisms of cationic phenylene ethynylene polymers and oligomers against *Escherichia coli*, Polymers (Basel, Switz.) 1 (2011) 3–6.
[35] M. Hartmann, M. Berditsch, J. Hawecker, M.F. Ardakani, D. Gerthsen, A.S. Ulrich, Damage of the bacterial cell envelope by antimicrobial peptides gramicidin S and PGLa as revealed by transmission and scanning electron microscopy, Antimicrob. Agents Chemother. 54 (2010) 3132–3142.
[36] S. Klayraung, S. Okonogi, Antibacterial and antioxidant activities of acid and bile resistant strains of *Lactobacillus fermentum* isolated from Miang, Braz. J. Microbiol. 757–766 (2009).
[37] E.R. Fischer, B.T. Hansen, V. Nair, F.H. Hoyt, D.W. Dorward, Scanning Electron Microscopy, 2012.